Design and Fabrication of Novel Ridge Guide Modulators in Lithium Niobate

Miguel García-Granda, Hui Hu, J. Rodríguez-García, and W. Sohler

***Abstract*—A thorough theoretical analysis of Mach–Zehnder-type ridge guide modulators has been performed in this paper. A novel electrode/waveguide structure was identified, yielding low driving voltages for high bandwidth operation. Based on this design, the fabrication of improved modulators was developed, introducing various novelties: low-loss Ti-indiffused wet-etched ridge guides in $LiNbO_3$, a complete ridge guide interferometer, and a specific electrode structure to be used with ridge interferometers. The operation of the modulator was demonstrated, yielding $V_\pi = 2.14$ V and $V_\pi L = 5.35$ V·cm at low frequencies and an ON–OFF extinction ratio of 20 dB.**

***Index Terms*—Electrooptic modulators, lithium niobate, ridge waveguides, wet etching.**

I. Introduction

External modulators based on lithium niobate ($LiNbO_3$) are key components for high-bit-rate optical communication systems due to their high modulation bandwidth, low insertion loss, low frequency chirp, and nearly wavelength-independent characteristics. Nowadays, commercial devices offer a modulation bandwidth (Δf), exceeding 40 GHz combined with a low driving voltage (V_π) in the range of 4–5 V, with a voltage-length product ($V_\pi L$) of the order of 12–15 V·cm at low frequencies.

Due to the limitations of electrical modulator drivers, lower drive voltages are essential to enable higher bit rates and reduce the cost of modulator operation. Therefore, the reduction of the driving voltage of $LiNbO_3$ modulators is an extremely important issue for realizing future high-speed optical transmission systems. Driving voltages in the range of 2 V are desired in order to use inexpensive SiGe drivers for high-bandwidth applications.

There has been a lot of work to develop modulator structures matching these requirements. For example, thin sheet approaches, in which layers of single crystalline $LiNbO_3$ of micrometer thickness are exploited, have been demonstrated [1]–[3]. Ferroelectric domain inversion (DI) in $LiNbO_3$ was also used in some designs to develop new electrode structures or tailor the electro-optical response [4]–[6]. Even folded interferometric structures have been proposed in order to reduce the size of the devices [7], [8].

Finally, slow light effects in photonic crystal structures have also been exploited in amplitude modulators to get a further miniaturization and reduce V_π [9].

A suitable technique for near-future industrial fabrication is the use of ridge waveguides. For experimental devices, it has been demonstrated that ridge waveguides can improve the modulator characteristics, leading to $V_\pi L$ of the order of 8–9 V·cm [10]–[12]. At the same time, the waveguide geometry and traveling-wave electrode can be optimized to get impedance matching and high-bandwidth performance [13].

In this paper, we present the results of a thorough modeling of ridge waveguide modulators in $LiNbO_3$. The outcome is a high-bandwidth design with a novel electrode/waveguide structure that further reduces V_π. By using advanced fabrication techniques, we were able to fabricate such modulators with a V_π of 2.14 V only and a $V_\pi L$ of 5.35 V·cm.

II. Fundamentals of Interferometric Modulators

In a Mach–Zehnder (MZ) interferometric modulator, the change in refractive index (Δn) in each waveguide of the interferometer is

$$\Delta n = -\frac{1}{2} n^3 r E \tag{1}$$

where E is the applied electric field by the electrodes and r is the relevant electro-optic coefficient. The best choice for $LiNbO_3$ is r_{33}, which is the highest one, and $n = n_e$, where n_e is the extraordinary refractive index.

As the field E is not homogeneous throughout the guided mode area, an overlap factor (Γ) must be introduced. This factor can be defined [14] as follows:

$$\Gamma = \frac{G}{V_0} \frac{\iint_\infty E_m(z,y)|E_{\rm opt}(z,y)|^2 dz\, dy}{\iint_\infty |E_{\rm opt}(z,y)|^2 dz\, dy} \tag{2}$$

where G is the gap between the electrodes (see Fig. 1), V_0 is the peak applied voltage, and E_m and $E_{\rm opt}$ are the modulating and optical fields, respectively.

The applied voltage needed in order to obtain a complete destructive interference is called the driving voltage (V_π), and depends on the interaction length (L) of the device. The relation

Manuscript received May 19, 2009; revised August 05, 2009. First published October 20, 2009; current version published November 25, 2009. This work was supported by the Spanish Ministerio de Educación y Ciencia under Project TEC2005-05541 and FPI Grant BES2004-4485, and in part by the Graduate College of the University of Paderborn.

M. García-Granda was with the Applied Physics/Integrated Optics Group, University of Paderborn, 33098 Paderborn, Germany. He is now with the Institute of Photonic Sciencies, 08860 Barcelona, Spain. (e-mail: miguel.garcia-granda@icfo.es).

H. Hu and W. Sohler are with the Applied Physics/Integrated Optics Group, University of Paderborn, 33098 Paderborn, Germany.

J. Rodríguez-García is with the Department, University of Oviedo, 33007 Oviedo, Spain.

Color versions of one or more of the figures in this paper are available online at http://ieeexplore.ieee.org.

Digital Object Identifier 10.1109/JLT.2009.2034756

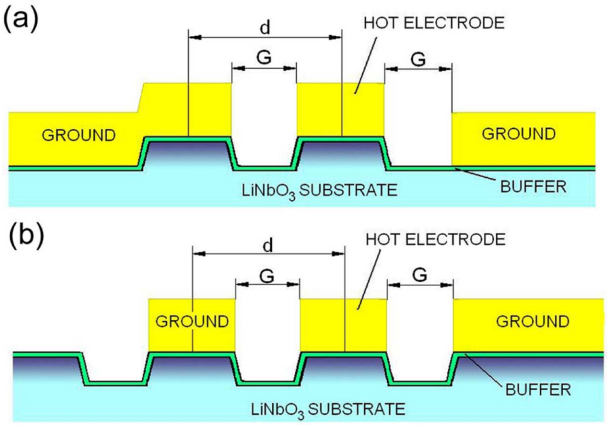

Fig. 1. Cross-sections of: (a) traditional CPW electrode structure on a ridge guide interferometer and (b) novel SACPW structure.

between both of them is called the voltage-length product and can be calculated as follows:

$$V_\pi L = \frac{\lambda G}{n^3 r \Gamma}. \tag{3}$$

In high-bandwidth modulators, the electrodes are designed as microwave (MW) waveguides. The best modulation efficiency is obtained when the modulating wave travels at the same velocity as the optical wave (velocity-matching condition). This means that the effective indexes of the MW signal $(n_{\text{eff}}^{\text{MW}})$ and the optical wave $(n_{\text{eff}}^{\text{op}})$ are equal. Moreover, the characteristic impedance of the electrodes (Z) should be, ideally, similar to the 50 Ω value used in MW circuitry and devices [15].

The frequency response of the device is also influenced by the MW loss generated both in the conductive and dielectric materials. The frequency dependence of this loss can be calculated as [16] follows:

$$\alpha(f) = \alpha_c + \alpha_d = \alpha_{c0}\sqrt{f} + \alpha_{d0} f \tag{4}$$

where α_{c0} and α_{d0} are, respectively, the conductor and dielectric loss parameters normalized at 1 GHZ, and f is the frequency. The frequency response can be calculated as function of the phase shift at DC, $\Delta\phi$ (DC), and a frequency $f, \Delta\phi(f)$, as [17]

$$m(f) = \left| \frac{\Delta\phi(f)}{\Delta\phi(\text{DC})} \right|. \tag{5}$$

III. Design of Ridge Guide Modulators

Previous attempts made with ridge in $LiNbO_3$ were based on partial etching of the substrate around the waveguides in the interaction area (along the parallel arms of the interferometer) [18], [19]. This allowed a reduction of $n_{\text{MW}}^{\text{eff}}$, thus improving the velocity matching.

However, the waveguides in previously reported ridge devices were fabricated by using diffusion techniques (typically, Ti in-diffusion or proton exchange), yielding a bidimensional graded index waveguide before the ridge fabrication [18], [19]. This approach was sometimes necessary to isolate the optical mode from the rough ridge walls. However, it does not make the best use of a ridge structure, as the lateral confinement of light is not completely achieved by the interface air–$LiNbO_3$.

Moreover, previous ridge modulators used traditional coplanar waveguide (CPW) electrode structures for guiding the MW modulating signal [12], [18], [20], which is not the optimum electrode design for a ridge structure.

In our approach, we introduce various technological novelties with the aim of improving modulator performance: low-loss and high-confinement Ti-indiffused ridge waveguides in $LiNbO_3$, a complete ridge guide interferometer, and a new electrode structure specifically designed for our ridge interferometers.

A. Ridge Waveguides

In order to achieve a strong reduction of $V_\pi L$, one needs to find, at the same time, the highest value for the overlap factor Γ and the smallest possible value for the gap between the electrodes G. To do this, the large mode profiles of indiffused waveguides (even indiffused index profiles inside a broad ridge) play a negative role, as they limit the minimum distance between parallel waveguides to prevent coupling.

Therefore, we propose the use of ridge waveguides in which the lateral confinement is created by the ridge walls, thus obtaining high confinement and reduced cross section. This requires a suitable fabrication process in which the wall roughness is reduced in order to prevent additional optical loss.

B. Complete Ridge Guide Interferometer

One important property of the ridge waveguides is that they potentially allow sharper waveguide bendings [21], which, used in an MZ-type interferometer, might also decrease the length of the Y-splitters. Moreover, preventing transitions between indiffused and ridge waveguides in the device reduces losses due to mode mismatch, and simplifies the fabrication process.

Therefore, our proposal is to develop a complete-ridge interferometer (with interaction section, Y-splitters, and input and output waveguides, all made of ridge waveguide) by adapting the recently developed methods to fabricate high-quality ridge waveguides in Ti:$LiNbO_3$ [22].

C. Electrode Structure

When implementing a traditional CPW electrode structure on a ridge modulator, the vertical component of the applied electric field (parallel to the Z crystal axis) is not optimally used. Moreover, nonnegligible values of horizontal electric field can be reached in the waveguides, giving place to undesired effects on the polarization of light.

Therefore, we introduce the surface-asymmetric CPW (SACPW) design (see Fig. 1), which includes three electrodes at the same level of the $LiNbO_3$ surface, whereas the ridge waveguides are defined by etched areas below the electrode. The signal electrode and one of the ground electrodes consist of narrow metal stripes with the same width as the ridges.

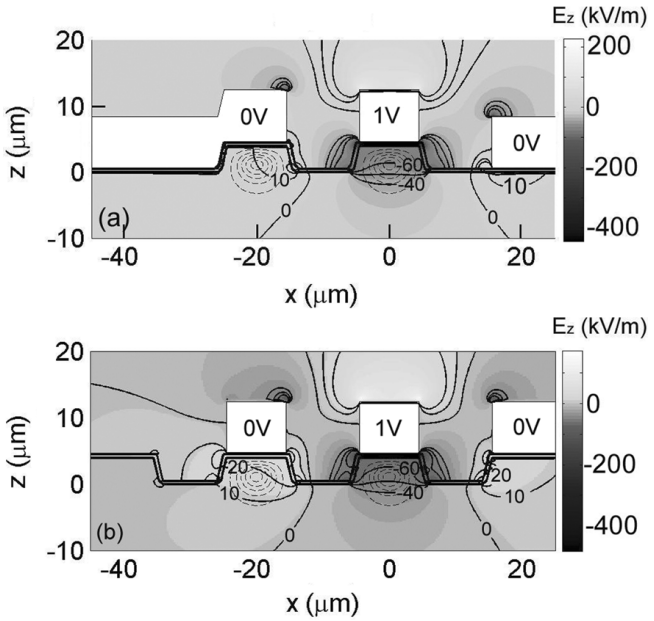

Fig. 2. Calculated distribution of optical modes and vertical component of electric field for (a) the CPW on ridge and (b) the SACPW structures. Distance between waveguide centers is 20 μm. Ridges are 9 μm wide and 4 μm high.

IV. Simulation Results

In order to calculate the performance of different modulator structures, the experimental waveguide geometry obtained by wet etching of Z-cut $LiNbO_3$ was taken into account [22]. As refractive index profile, we used the one obtained by the diffusion of a Ti stripe of the same width as the ridge into a planar substrate and neglected the part of the diffusion profile beyond the ridge walls [23]. Comparison of calculated modes based on this model with measured mode distributions in ridge waveguides showed a good agreement.

A finite-difference method was used to calculate the quasi-static distribution of optical and electrical fields in the cross section of the modulator. From these data, the key modulator parameters ($V_\pi L, n_{\text{eff}}^{\text{MW}}$, and Z) were calculated.

Fig. 2 shows the cross sections of CPW on ridge and SACPW modulators as seen in the simulations. The optical mode profiles are depicted by thin dashed lines. The gray scale and numerical labels show the amplitude of the vertical component of the applied electric field (E_z) when a voltage of 1 V is applied between the electrodes. It is evident that the SACPW produces a more symmetric distribution of the electric field and improves its overlap with the optical modes. In this way, both waveguides receive a higher electric field, and the chirp effect of the modulator is reduced.

In order to analyze the performance of the ridge devices, the modulator characteristics ($V_\pi L, n_{\text{eff}}^{\text{MW}}$, and Z) were calculated for the proposed SACPW structure as a function of the ridge height (h) and taking the distance between waveguides, d, and the electrode and buffer layer thicknesses, t_e and t_b, as parameters. The results are shown in Fig. 3.

In Fig. 3(a), we observed that there is an optimum ridge height around 4 μm, which agrees with previous calculations made for other types of ridge structures [16]. In this calculation, different values of electrode thickness were omitted as they do not change

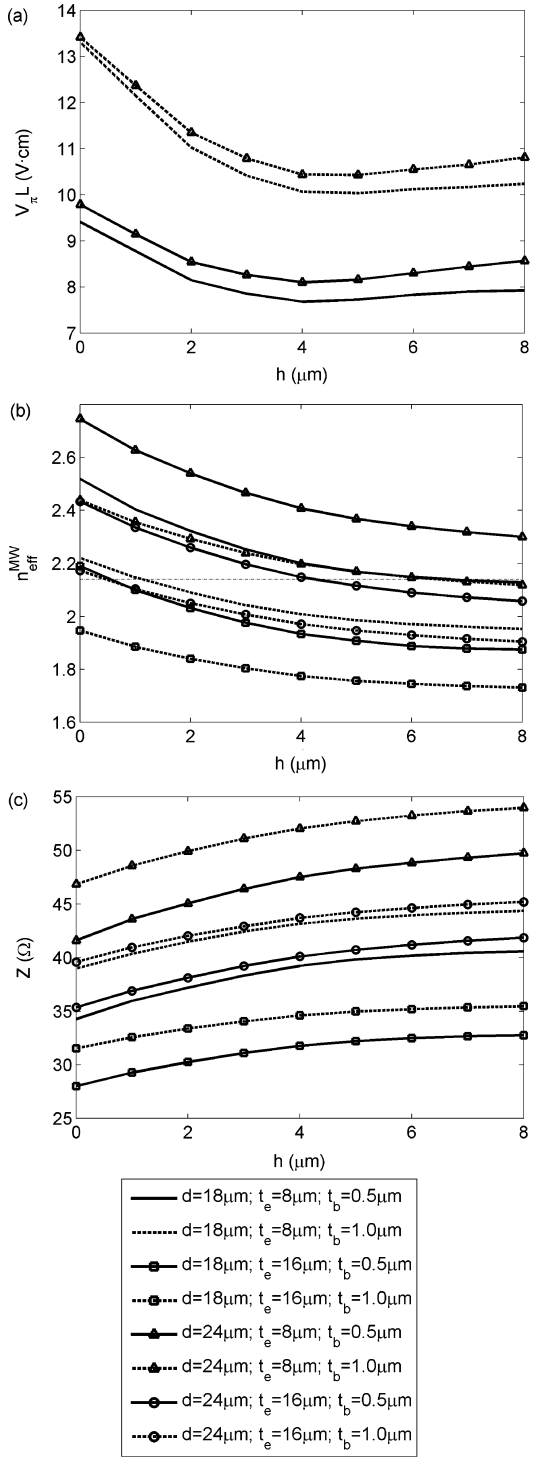

Fig. 3. Calculated modulator characteristics of the proposed SACPW structure: (a) driving voltage-length product; (b) effective index of the modulating microwave; and (c) characteristic impedance. In (b), the optical effective index is depicted as a dashed horizontal line at $n_{\text{eff}}^{\text{MW}} = n_{\text{eff}}^{\text{op}} = 2.14$.

the result significantly. It is clear that the thinner the buffer layer is, the lower the driving voltage becomes. In this way, the higher voltage imposed by a structure with more separated waveguides can be notably compensated if a thinner buffer layer can be used.

In Fig. 3(b), we observed that the effect of ridge height is to reduce the value of $\text{n}_{\text{eff}}^{\text{MW}}$. In order to get velocity matching (marked by the dashed horizontal line) around $h = 4$ μm, one

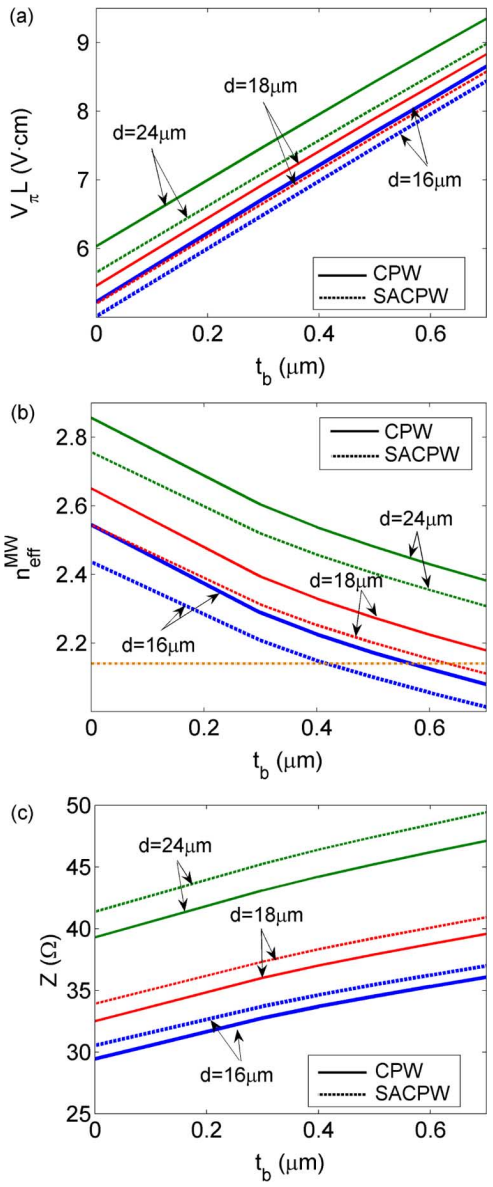

Fig. 4. Calculated modulator parameters as function of the buffer layer thickness (t_b) for the SACPW and CPW on ridge structures as depicted in Fig. 1.

of the best options is the use of a small distance d (18 μm) with thin buffer layer (around 0.6 μm) and relatively thin electrodes (8 μm). An alternative is the use of higher distance (24 μm), but this requires either the use of thick buffer layer (1 μm or more) or thicker electrodes, which also implies a more complicated and sensitive fabrication process.

Fig. 3(c) shows that the ridge height contributes to the increase of impedance, so as the buffer layer does. The closest values to 50 Ω are obtained when larger distance d is used. However, the impedance mismatch is usually mitigated by using tapered electrodes and matched terminations.

Based on these results, we can now compare the performance of the proposed SACPW structure with the traditional CPW electrode on ridge, both with a ridge height of 4 μm. This can be seen in Fig. 4 as a function of the buffer layer thickness (t_b). For these calculations, the distance between waveguide centers (d) has been taken as a parameter and t_e has been set to 8 μm. A waveguide and electrode width of 9 μm was chosen as a best tradeoff between low optical loss and high optical mode confinement [24].

Fig. 4(a) shows the voltage-length product, $V_\pi L$, as a function of the buffer layer thickness. One can see that the SACPW structure reduces the $V_\pi L$ by about 5% in comparison with the CPW structure for the same geometry. As we may expect, the smaller the distance d is, the lower the $V_\pi L$ results. Nevertheless, a minimum separation is needed in order to prevent coupling between waveguide modes. Values of d in the range of 16 to 20 μm would already result in coupling of conventional diffused waveguides.

In Fig. 4(b), we observed that a significant improvement is provided by the SACPW structure in which, for t_b between 0.5 and 0.7 μm, the MW index matches the optical index ($n_e = 2.14$, shown in the graph as a horizontal dashed line). It can be seen that velocity matching can be obtained with thinner buffer layer for SACPW than for CPW, which means that the driving voltage of the final device will be lower.

Fig. 4(c) shows the impedance as a function of t_b with d as parameter. When the SACPW structure is used, the impedance values are higher and closer to 50 Ω. Nevertheless, shorter d means a lower value of Z, which is not ideal. However, as aforementioned, one can reduce the influence of the Z mismatch by using a proper tapering of electrodes and matched terminations. Therefore, the most critical device parameters, $V_\pi L$ and $n_{\text{eff}}^{\text{MW}}$, are notably improved by the ridge structure and, in particular, the SACPW design.

Another important issue related to the electrode design is the losses that it can produce both in the optical signal and the MW signal.

We saw that the ridge structure (and, in particular, the SACPW design) allows to obtain velocity matching with thinner buffer layer than conventional designs. This is advantageous as it improves the attainable values of $V_\pi L$. Nevertheless, one should also note that a minimum buffer thickness is necessary in order to prevent optical losses at the conductor. To get an idea about that loss in our designs, we used a finite-elements method to compute the optical mode profile, taking into account the proximity of a conductor and evaluating the imaginary part of the resulting modal propagation constant. The result can be seen in Fig. 5, from which we can conclude that values of t_b beyond 0.5 μm provide a negligible optical loss (in the order of 10^{-5} dB/cm) in comparison with the rest of sources of optical loss such as fiber-to-waveguide mode mismatch, surface roughness, wall roughness (in the case of ridge waveguides), loss at Y-junctions (in interferometers), irregularities in Ti concentration, or intrinsic defects of the substrate. This is also reasonable due to the fact that the high index contrast between the $LiNbO_3$ and the SiO_2 (2.14 and 1.44, respectively, at 1.55 μm wavelength) creates a high confinement, such that the optical field does not penetrate the buffer layer beyond, roughly, 100 nm.

The conductor losses in the MW transmission line shown in (4) can be calculated by using Wheeler's rule as [15], [25]

$$\alpha_{c0} = \sqrt{\frac{\pi\mu_0}{\sigma}}\frac{\varepsilon_0}{Z_0}\left(\frac{\partial}{\partial G} - \frac{\partial}{\partial W} - \frac{\partial}{\partial t_e}\right)\frac{1}{C_0} \qquad (6)$$

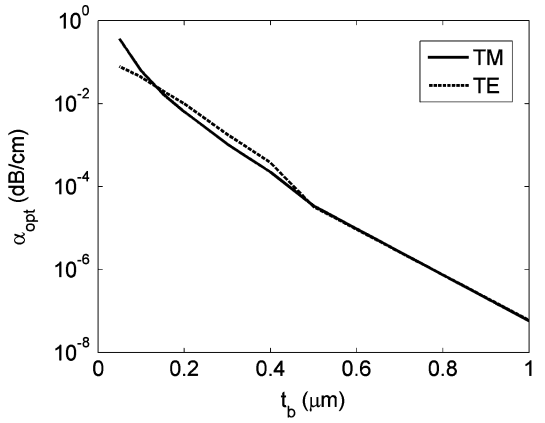

Fig. 5. Calculated optical loss due to the electrode as function of the buffer layer thickness (t_b) for the TE and TM modes in a Ti indiffused waveguide.

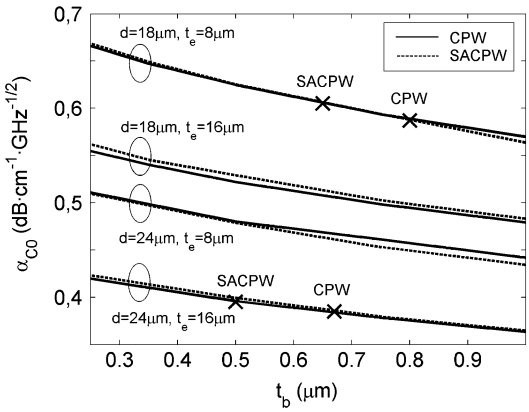

Fig. 6. Calculated conductor loss as a function of the buffer layer thickness with the distance between waveguide centers and electrode thickness as parameters. Velocity-matching conditions for each design are marked with X.

where σ is the conductivity of the electrode, Z_0 and C_0 are, respectively, the impedance and the capacitance of the electrode in vacuum, G is the electrode gap, W is the electrode width, and t_e is the electrode thickness. The result of the calculation applied to SACPW and CPW structures can be seen in Fig. 6.

In Fig. 6, we observed that the conductor loss for both types of electrodes is very similar. For comparison, two pairs of points have been highlighted, which represent the value of t_b necessary to obtain velocity matching in each configuration. We see that, in the velocity-matching condition, the SACPW implies an increase in loss of, approximately, only 3%.

The dielectric losses can be calculated as [17] follows:

$$\alpha_{d0} = \frac{\pi}{cn_{\text{eff}}^{\text{MW}}}(\Gamma_{\text{LN}}\varepsilon_{LN}\ \tan\delta_{\text{LN}} + \Gamma_b\varepsilon_b\ \tan\delta_b) \qquad (7)$$

where Γ_i are the confinement factors of MW power in each material ($LiNbO_3$ or SiO_2 buffer), ε_i are the relative dielectric constants, and $\tan\delta_i$ are the loss tangents, which take typical values of 10^{-3} for $LiNbO_3$ and 5×10^{-3} for SiO_2 [26]. By doing these calculations, typical values of α_{d0} were found in the range

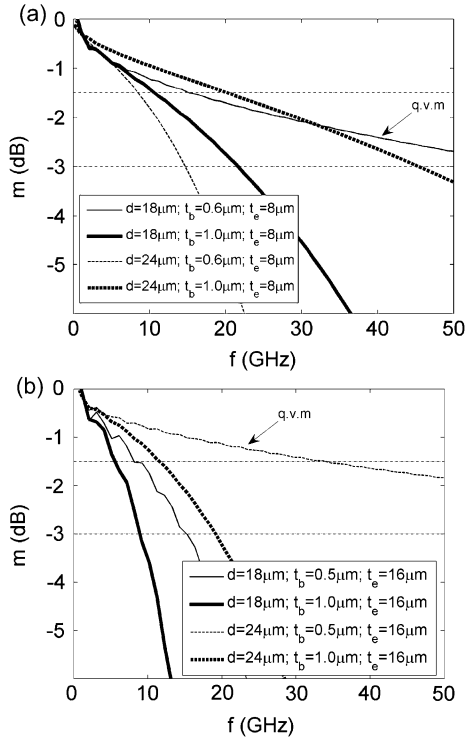

Fig. 7. Calculated frequency response for the SACPW modulator structure using d, t_b, and t_e as parameters. Optical 3 dB level is shown (horizontal dashed line at -3 dB level), as well as the electrical 3 dB threshold (shown at -1.5 dB level).

4×10^{-3} to 9×10^{-3} dB·cm^{-1}·GHz^{-1}. Obviously, the dominant influence in the modulation performance will be that of the conductor losses up to frequencies around 40 GHz [27].

Taking into account the results found for the SACPW structure, the frequency response $[m(f)]$ was calculated using (5) and evaluating the effective voltage along the electrodes using a method similar to that described in [17]. The calculation was applied to devices with $t_e = 8\ \mu$m [see Fig. 7(a)] and $t_e = 16\ \mu$m [see Fig. 7(b)], with an active length (L) of 25 mm.

In both graphs, a case with quasi-velocity matching was included. On one side, $d = 18\ \mu$m and $t_b = 0.6\ \mu$m for $t_e = 8\ \mu$m (which provides $V_\pi L = 8.17$ V·cm and $V_\pi = 3.27$ V), and on the other side, $d = 24\ \mu$m and $t_b = 0.5\ \mu$m for $t_e = 16\ \mu$m (which provides $V_\pi L = 8.12$ V·cm and $V_\pi = 3.25$ V). These cases are highlighted in the figure with the label q.v.m. Also cases with the same parameters and $t_b = 1\ \mu$m were included for sake of comparison with nonvelocity matched designs.

From these results, we see that high-speed devices with low driving voltage and a 3 dB optical bandwidth beyond 40 GHz can be obtained when velocity-matching conditions are fulfilled. One of the greatest advantages of the proposed ridge structure in this case is the ability to obtain velocity matching with thin buffer layers, which notably improves the driving voltage for high-bandwidth devices. On the other side, we can see that the possibility of using small separation between waveguide centers (e.g., 18 μm) provides the chance to obtain velocity matching with thin electrodes (8 μm). This fact can be an advantage from the technological point of view as the processes involved in thinner electrodes fabrication are less sensitive and provide easier fabrication.

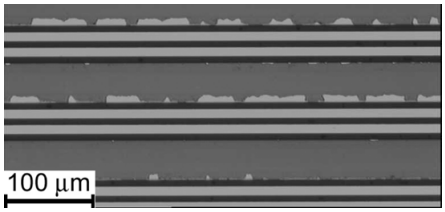

Fig. 8. Micrograph of a ridge sample in which self-alignment technique was performed to coat the top of the interferometer ridges with Ti. The Ti layer is seen in light gray, the $LiNbO_3$ is seen in dark gray, and the bottom of the etched grooves is seen in black.

V. Modulator Fabrication

Based on the results obtained from the simulations, and applying advanced fabrication techniques developed by us, we fabricated SACPW modulators using $L = 25$ mm and the geometric parameters given before.

An e-beam written mask is used to transfer the interferometer pattern to a Cr layer (100 nm thick) deposited on the surface of the $-Z$ face of $LiNbO_3$. Then, the Cr mask is annealed at 300 °C for 3 h in order to improve its adhesion. By a wet etching process in a mixture of HF, HNO_3, and ethanol, the ridge structure is fabricated [22]. The samples are etched with vigorous stirring at a constant temperature of 20.0 ± 0.5°C, which gives an etching rate of, approximately, 0.5 μm/h. After the desired depth is reached (3 to 4 μm), the ridge structure is thoroughly cleaned using an RCA-1 process and then coated with photoresist (OIR907-17). Then, a short-time flood exposure with UV light is made. If the exposure and development times are accurately chosen, only the photoresist on top of the ridges will be removed, and it will remain at the bottom of the etched parts and on top of the lateral planes (typical times are around $1/3$ of the time used to completely expose and develop the same photoresist on a planar substrate). Then, the samples are coated with a 70 nm-thick Ti layer and a liftoff is made. This leaves a Ti strip covering only the top of the ridges. Subsequently, the Ti in-diffusion is performed. This self-alignment process, which will be further described and applied to different devices in a forthcoming publication [28], has two advantages. On one side, there is no need for an additional lithographic alignment step, which reduces the fabrication cost and time. On the other side, the in-diffusion process after wet etching reduces the roughness of the walls and leads to a decrease of optical losses. This is fundamental if a strong light confinement is desired, which is of capital importance in order to obtain the maximum performance of ridge structures.

Fig. 8 shows a micrograph of a sample after the self-alignment process in which only the ridges of three parallel interferometers are coated with Ti.

In Fig. 9, SEM images of a fabricated sample are shown.

Fig. 9(a) shows the splitting point of a ridge Y-splitter made with an angle of 0.34° between the output waveguides. In Fig. 9(b), the section of the parallel waveguides that form the interferometer arms can be seen. The SiO_2 buffer layer is clearly visible in this micrograph.

The fabrication of electrodes proved to be a great challenge, due to the areas where the electrodes have to cross the etched

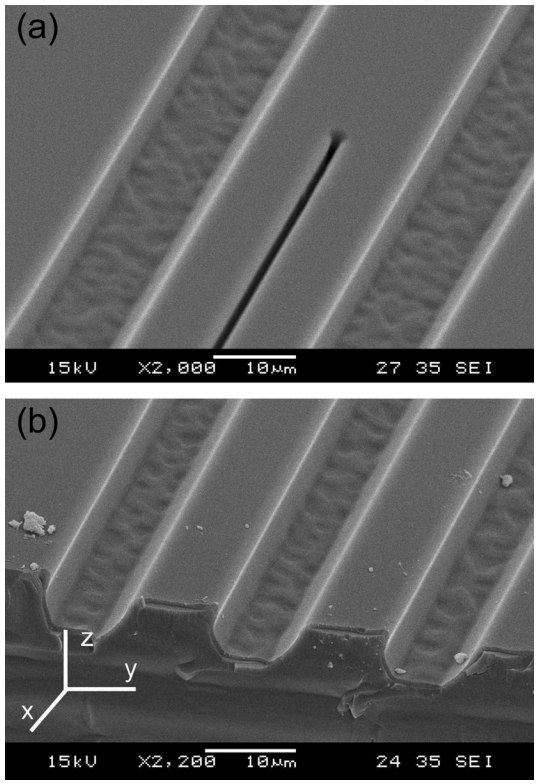

Fig. 9. SEM images of (a) a ridge-waveguide Y-splitter in a fabricated SACPW modulator at the point where the two interferometer waveguides split and (b) the parallel waveguides in the interferometer coated with a 0.5 μm-thick SiO_2 buffer layer. The orientation of the crystal axes is shown in (b).

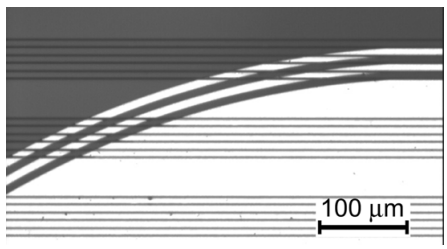

Fig. 10. Micrograph of the fabricated SACPW electrodes (white) on a sample with several ridge interferometers.

grooves. Fig. 10 shows three sets of parallel ridge waveguides in the horizontal direction, corresponding to three independent interferometers. The electrodes are seen in white, performing a bend to reach the interferometer to be addressed, which is the upper one. At the top right corner, the electrodes are already aligned with the ridge waveguides at the point where the interaction length begins.

Usually, thick electrodes for MW applications are fabricated by using electroplating. This process needs a thin Au coating of the sample as precursor for the Au electrodeposition. Afterwards, a thick resist shapes the electrodes during the plating process, and finally, the thin layer is etched in order to open the gaps between the thick electroplated electrodes.

This etching procedure was very difficult to perform due to the wall shape. A short circuit between electrodes was usually found, created by metal deposits formed at the bottom of the grooves near the base of the ridges. Even the buffer layer below

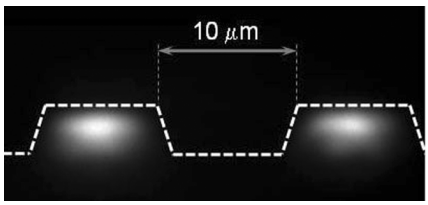

Fig. 11. Optical profile of modes guided by interferometer arms in the cross section of the device. The profile of the ridge structure is depicted as a dashed line.

the Au was sometimes damaged before the metal could be completely etched by inductively coupled plasma (ICP) etching. For this reason, a liftoff technique was chosen to successfully fabricate 2 μm-thick evaporated Au electrodes in order to test the low-frequency performance.

Nevertheless, this technique is not compatible with a traditional electroplating process. The way to create thick electrodes in these and similar structures is being studied by the authors and will be presented in the near future.

VI. Modulator Characterization

The loss of fabricated waveguides was measured using a Fabry–Perot resonance setup [29]. For a waveguide width between 8 and 9 μm, and 3 μm height, the typical losses were 0.5 ± 0.1 dB/cm for the TM mode and 0.15 ± 0.05 dB/cm for the TE mode. These results match the sequence published in [22] for narrower waveguides. The full-width at half-maximum (FWHM) of the TM mode was 4.3 and 3.3 μm in the horizontal and vertical directions, respectively. Broader waveguides showed lateral multimode behavior, which is not suited for an interferometric modulator.

The typical insertion loss of our devices, measured via fiber butt-coupling, was in the range of -10 dB. Considering the loss of straight waveguides, the excess loss induced by the Y-junctions and bendings was around 8 dB.

Fig. 11 shows the profile of both modes guided by the interferometer arms in a cross section of the structure. It becomes obvious that a waveguide separation of only 10 μm is more than sufficient to prevent mode coupling. Even smaller separations would be possible in order to further reduce the driving voltage. However, one should take into account the resulting reduction of electrode impedance [see Fig. 2(c)].

In Fig. 12, the electro-optic response of a modulator with $d = 18$ μm, $t_b = 0.5$ μm, and $h = 3.5$ μm is shown when a 1 kHz triangular signal is applied. The obtained driving voltage is 2.14 V and the extinction ratio is 20 dB. As the interaction length of fabricated samples is 25 mm, the obtained $V_\pi L$ is 5.35 V·cm.

According to the calculations, this configuration would provide a Δf greater than 30 GHz if the proper thick electrodes were implemented.

Samples with a ridge height lower than 3 μm were multimode, showing the first horizontal higher order mode, due to the diffusion of Ti into the substrate beyond the lateral walls. This

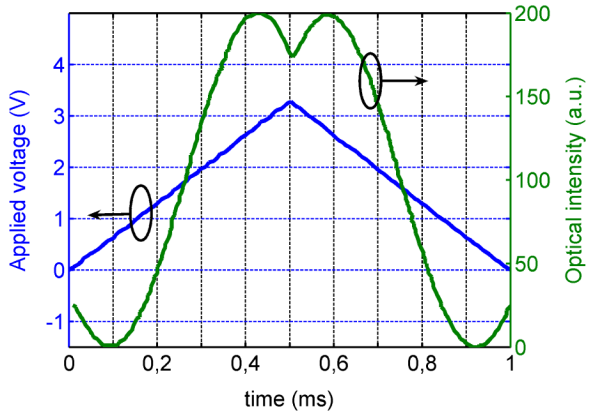

Fig. 12. Measured optical intensity output and applied voltage as function of time. A driving voltage of $V_\pi = 2.14$ V results from this measurement.

fact dramatically decreased the modulator performance. Therefore, ridge heights above 3 μm are needed when using this fabrication technology and the parameters given before. In devices with a ridge height between 3 and 4.5 μm, no significant dependence of the driving voltage on the ridge height was found.

According to Fig. 12, the lower value of $\mathrm{V_\pi L}$, in comparison with the calculation results, might be due to the nonideal modeling of the Ti in-diffusion and, therefore, the refractive index profile.

VII. Conclusion

An extensive theoretical investigation of MZ-type ridge guide modulators has been done. A novel SACPW structure was identified to yield lower driving voltage and higher bandwidth than conventional CPW designs on ridge and planar substrates.

Such a modulator, consisting of a complete ridge structure, including Y-junctions and input and output waveguides, has been developed. Novel fabrication techniques of high-confinement and low-loss ridge waveguides, as well as a self-alignment technique were applied with the aim of simplifying the fabrication process. Thin electrodes were fabricated in order to measure the low-frequency behavior.

The complete fabrication process was developed and discussed, and critical issues were analyzed. Finally, fabricated modulators were characterized, yielding a $V_\pi = 2.14$ V, a $V_\pi L$ of 5.35 V·cm, and an ON-OFF extinction ratio of 20 dB when driven by a low-frequency signal. These results are substantially better than the parameters of commercial modulators as well as previously published results.

The characterization was limited to low frequencies due to the difficulties encountered in the electrode fabrication on this ridge structure. Nevertheless, the authors are currently developing an electrode fabrication process, overcoming the existing problems.

Acknowledgment

The authors would like to thank S. Fernández, H. Herrmann, V. Quiring, R. Ricken and H. Suche for their contributions to this work.

REFERENCES

[1] K. Aoki, J. Kondo, A. Kondo, T. Mori, Y. Mizuno, S. Shimadaira, M. Imaeda, Y. Kozuka, O. Mitomi, and M. Minakata, "High performance optical modulator with a wide center electrode and thin X-cut $LiNbO_3$ substrate," *IEEE Photon. Technol. Lett.*, vol. 16, no. 12, pp. 2610–2612, Oct. 2004.

[2] P. Rabiei and W. H. Steier, "Lithium niobate ridge waveguides and modulators fabricated using smart guide," *Appl. Phys. Lett.*, vol. 86, pp. 161115-1–161115-3, 2005.

[3] G. Poberaj, M. Koechlin, F. Sulser, A. Guarino, J. Hajfler, and P. Günter, "Ion-sliced lithium niobate thin films for active photonic devices," *Opt. Mater.*, vol. 31, no. 7, pp. 1054–1058, 2009.

[4] F. Lucchi, D. Janner, M. Belmonte, S. Balsamo, M. Villa, S. Giurgola, P. Vergani, and V. Pruneri, "Very low voltage single drive domain inverted $LiNbO_3$ integrated electro-optic modulator," *Opt. Exp.*, vol. 15, no. 17, pp. 10739–10743, 2007.

[5] N. Courjal, H. Porte, J. Hauden, P. Mollier, and N. Grossard, "Modeling and optimization of low chirp $LiNbO_3$ Mach-Zehnder modulators with an inverted ferroelectric domain section," *J. Lightw. Technol.*, vol. 22, no. 5, pp. 1338–1343, May 2004.

[6] D. Janner, M. Belmonte, and V. Pruneri, "Tailoring the electrooptic response and improving the performance of integrated $LiNbO_3$ modulators by domain engineering," *J. Lightw. Technol.*, vol. 25, no. 9, pp. 2402–2409, 2007.

[7] W. K. Burns, M. M. Howerton, R. P. Moeller, A. S. Greenblatt, and R. W. McElhanon, "Broad-band reflection traveling-wave $LiNbO_3$ modulator," *IEEE Photon. Technol. Lett.*, vol. 16, no. 6, pp. 805–806, Jun. 1998.

[8] K. Aoki, J. Kondo, Y. Iwate, A. Hamajima, T. Ejiri, O. Mitomi, and M. Minakata, "High-speed X-cut thin sheet $LiNbO_3$ optical modulator with folded structure," *J. Lightw. Technol.*, vol. 25, no. 7, pp. 1805–1810, Jul. 2007.

[9] M. Roussey, M. P. Bernal, N. Courjal, D. V. Labeke, and F. I. Baida, "Electro-optic effect exaltation on lithium niobate photonic crystals due to slow photons," *Appl. Phys. Lett.*, vol. 89, pp. 241110-1–241110-3, 2006.

[10] O. Mitomi, K. Noguchi, and H. Miyazawa, "Design of ultra-broadband $LiNbO_3$ optical modulator with ridge structure," *IEEE Microw. Theory Tech.*, vol. 43, no. 9, pp. 2203–2207, Sep. 1995.

[11] S. Chang, C. Tsai, Y. Lin, J. Liu, and W. Wang, "Improved electrooptic modulator with ridge structure in X-cut $LiNbO_3$," *J. Lightw. Technol.*, vol. 17, no. 5, pp. 843–847, May 1999.

[12] W. K. Burns, M. M. Howerton, R. P. Moeller, R. Krähenbühl, R. W. McElhanon, and A. S. Greenblatt, "Low drive voltage, broad-band $LiNbO_3$ modulators with and without etched ridges," *J. Lightw. Technol.*, vol. 17, no. 12, pp. 2551–2555, Dec. 1999.

[13] M. García-Granda, H. Hu, W. Sohler, and J. Rodríguez-García, "Novel structures for broadband electrooptic modulators in $LiNbO_3$," presented at the Eur. Conf. Integr. Opt. (ECIO 2008), Eindhoven, The Netherlands, Jun. 11–13, 2008, Paper WeD4.

[14] C. M. Kim and R. V. Ramaswamy, "Overlap integral factors in integrated optic modulators and switches," *J. Lightw. Technol.*, vol. 7, no. 7, pp. 1063–1070, Jul. 1989.

[15] H. Chung, W. S. C. Chang, and E. L. Adler, "Modeling and optimization of traveling wave $LiNbO_3$ interferometric modulators," *IEEE J. Quantum Electron.*, vol. 27, no. 3, pp. 608–617, Mar. 1991.

[16] S. Haxha, B. M. A. Rahman, and K. T. V. Grattan, "Bandwidth estimation for ultra-high-speed lithium niobate modulators," *Appl. Opt.*, vol. 42, no. 15, pp. 2674–2682, 2003.

[17] N. Dagli, *High Speed Photonic Devices*. Boca Raton, FL: CRC Press, 2006, ch. 4.

[18] K. Noguchi, O. Mitomi, H. Miyazawa, and S. Seki, "A broadband Ti:$LiNbO_3$ optical modulator with a ridge structure," *J. Lightw. Technol.*, vol. 13, no. 6, pp. 1164–1168, Jun. 1995.

[19] K. Noguchi, O. Mitomi, and H. Miyazawa, "Millimiter-wave Ti:$LiNbO_3$ optical modulators," *J. Lightw. Technol.*, vol. 16, no. 4, pp. 615–619, Apr. 1998.

[20] M. M. Howerton, R. P. Moeller, A. S. Greenblatt, and R. Krähenbühl, "Fully packaged, broad-band $LiNbO_3$ modulator with low drive voltage," *IEEE Photon. Technol. Lett.*, vol. 12, no. 7, pp. 792–794, Jul. 2000.

[21] N. Anwar, S. S. A. Obayya, S. Haxha, C. Themistos, B. M. A. Rahman, and K. T. V. Grattan, "The effect of fabrication parameters on a ridge Mach-Zehnder Interferometric (MZI) modulator," *J. Lightw. Technol.*, vol. 20, no. 5, pp. 854–861, May 2002.

[22] H. Hu, R. Ricken, W. Sohler, and R. B. Wehrspohn, "Lithium niobate ridge waveguides fabricated by wet etching," *IEEE Photon. Technol. Lett.*, vol. 19, no. 6, pp. 417–419, Mar. 2007.

[23] E. Strake, G. P. Bava, and I. Montrosset, "Guided modes of Ti:$LiNbO_3$ channel waveguides: A novel quasi-analytical technique in comparison with the scalar finite-element method," *J. Lightw. Technol.*, vol. 6, no. 6, pp. 1126–1135, Jun. 1988.

[24] M. García-Granda and H. Hu, "Design of broadband electrooptical modulators using Ti:$LiNbO_3$ ridge waveguides," presented at the 5th Spanish Meeting Optoelectron. (OPTOEL 2007), Bilbao, Spain, Jul. , Paper MOI-13.

[25] K. C. Gupta, R. Carg, and I. J. Bahl, *Microstrip Lines and Slotlines*. Norwood, MA: Artech House, 1979.

[26] R. Yang and Y. Su, "Characteristics of coplanar waveguide on lithium niobato crystals as a microwave substrate," *J. Appl. Phys.*, vol. 101, pp. 014101-1–014101-5, 2007.

[27] K. Noguchi, H. Miyazawa, and O. Mitomi, "Frequency-dependent propagation characteristics of coplanar waveguide electrode on 100 GHz Ti:$LiNbO_3$ optical modulator," *Electron. Lett.*, vol. 34, no. 7, pp. 661–662, 1998.

[28] H. Hu, "Self-aligned metal-deposition on ridge structures for diffusion doping and electrode definition," submitted for publication..

[29] R. Regener and W. Sohler, "Loss in low-finess Ti:$LiNbO_3$ optical waveguide resonators," *Appl. Phys. B, Photophys. Laser Ch*, vol. 36, pp. 143–147, 1985.

Miguel García-Granda received the degree in physics from the University of Oviedo, Oviedo, Spain, in 2003, and the Ph.D. degree from the University of Oviedo and the University of Paderborn, Paderborn, Germany, in 2009.

During 2003, he joined Hanh-Meitner Institut, Berlin, Germany, where he was involved in solar cells fabrication and characterization technologies. His research work was focused on lithium niobate electrooptic modulators based on ridge waveguides. Currently, he is with the Institute of Photonics Sciences, Barcelona, Spain, where he is engaged in the field of micro-engineered electrooptical devices and sensors.

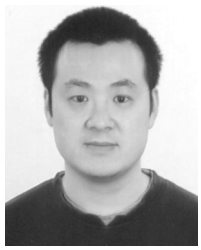

Hui Hu received the Bachelor's and Ph.D. degrees in physics from Shandong University, Beijing, China, in 1996 and 2001, respectively.

During 2001, he was with the Electronic Engineering Department, Tsinghua University, China, where he was engaged in research on metalorganic chemical vapour deposition epitaxial growth of Group III-Nitrides. During 2004, he was with the Physics Department, University of Paderborn, Paderborn, Germany, as an Alexander von Humboldt (AvH) Research Fellow, where he is currently with the Applied Physics/Integrated Optics Group. "His research interest is focused on the high-refractive-index-contrast single-crystalline $LiNbO_3$ thin films and corresponding devices.

J. Rodríguez-García photograph and biography not available at the time of publication.

W. Sohler photograph and biography not available at the time of publication.